Journal of Materials Research and Technology 41 (2026) 1353–1367

Contents lists available at ScienceDirect

Journal of Materials Research and Technology

journal homepage: www.elsevier.com/locate/jmrt

Investigation of machining parameters and cooling strategies on the burr geometry in micro-milling of titanium alloy (Ti–6Al–4V)

Gulfam Ul Rehman [a], Muhammad Rizwan ul Haq [a,*], Syed Husain Imran Jaffery [b], Muhammad Salman Khan [a], Shahid Ikramullah Butt [a]

[a] Department of Design and Manufacturing Engineering (DME), School of Mechanical and Manufacturing Engineering (SMME), National University of Sciences and Technology (NUST), Sector H-12, Islamabad, 44000, Pakistan

[b] School of Engineering and the Built Environment, Faculty of Computing, Engineering and the Built Environment, Birmingham City University, Birmingham, B4 7XG, UK

ARTICLE INFO

Keywords:
Micro-milling
Ti–6Al–4V
Precision machining
Cutting speed ranges
Burr formation
Cooling strategies

ABSTRACT

Titanium-based alloys are indispensable in aerospace, biomedical, automotive, and marine applications due to their exceptional strength-to-weight ratio, high-temperature capability, biocompatibility, and corrosion resistance. However, micro-milling of Ti–6Al–4V is prone to burr formation, which necessitates post-processing that can damage delicate micro-features and compromise dimensional fidelity. This study systematically compares burr formation across conventional, transition, and high-speed cutting ranges under different cooling strategies and statistically quantifies how feed per tooth, cutting speed, depth of cut, and cooling govern burr width and height on the up and down-milling sides. Micro-milling experiments varied these factors; burr metrics were measured and analyzed using a variance-based contribution approach. Results show that across the three speed ranges, the transition-speed window yielded the most favorable outcomes, with minimum burr at $V_c \approx 75$ m/min. Burr width was governed mainly by feed per tooth and cutting speed, both inversely related to width; their combined contribution ranged from 82 to 89 % (up-milling) and 69–92 % (down-milling). Burr height was dominated by depth of cut and feed per tooth; each directly related to height; their combined contribution ranged from 77 to 90 % (up-milling) and 74–85 % (down-milling). Under the optimized parameters, burr width decreased by 19 % (up-milling) and 9 % (down-milling), and burr height decreased by 25 % in both milling directions.

1. Introduction

Micro-machining produces highly miniaturized parts and features [1,2], meeting the increasing demand for precision and accuracy in industries such as communication, optics [3], biomedical [1,3], electronics, aerospace, and automotive. The trend towards miniaturization is rapidly growing in these fields due to the potential benefits it offers in terms of enhanced healthcare, quality of life, and economic growth [1,4]. In this context, micro-milling has emerged as an advanced machining technique capable of producing intricate three-dimensional (3D) miniaturized components and features [5–8]. Micro-milling is often preferred over other non-traditional machining processes due to its high material removal rate, process flexibility, lower setup costs [5,7], and ability to produce intricate shapes [2].

Despite these advantages, micro-milling faces several challenges, including burr formation, surface quality issues, rapid tool wear, and unpredictable tool breakage [5,7]. Because of this, factors often negligible at the macro scale such as tool vibration [1,9], subsurface plastic deformation [1], and material microstructure [9], become important in micro-level machining. Micro-milling presents significant challenges when working with hard-to-cut materials, such as the Ti–6Al–4V titanium alloy [7]. Ti–6Al–4V is widely recognized as the foundational alloy of the titanium industry due to its versatile applications and balanced mechanical properties [1,10], and it represents over 50 % of titanium usage [11]. This alloy is widely used in the aerospace industry [9,10,12] for aircraft engines [12] and turbine blades and fasteners [3,9,13], in the automotive sector [10,14,15] for components like connecting rods, engines, and exhaust valves [14], micro-channels in heat exchangers, micro-pillars [12], military equipment [12,16], and marine industry [16,17].

Despite its superior properties, the alloy's low thermal conductivity [9,18,19], high chemical reactivity [19,20], low elastic modulus [20,21]

* Corresponding author.
E-mail address: muhammad.rizwan@smme.nust.edu.pk (M.R. Haq).

https://doi.org/10.1016/j.jmrt.2025.12.121
Received 28 April 2025; Received in revised form 18 November 2025; Accepted 11 December 2025
Available online 13 December 2025

and high hardness at elevated temperatures [21] make it difficult to machine [9,21]. Mechanical machining, whether on a macro or micro scale, invariably leads to burr formation. However, deburring presents greater challenges in micro-machining compared to macro-machining. In micro-components, the deburring process poses a risk of damaging the workpiece and compromising delicate micro-features. Additionally, deburring is costly due to the complex assembly operations required [18,22]. Therefore, employing a deburring process to remove burrs is generally not recommended. Instead, the recommended approach is to optimize machining parameters and tool geometry to minimize burr formation [9].

1.1. Tool parameters and burr mechanisms

Burr formation in micro-milling is governed first by feed per tooth (f_z) relative to tool edge radius (r_e). When the undeformed chip thickness is below the edge radius, rubbing and ploughing dominate and burr size increases; when f_z exceeds r_e, shearing stabilizes and burr formation decreases. This transition was established in early research on micro-milling and confirmed for Ti–6Al–4V, where feed emerged as the dominant factor and very low feeds increased variability through vibration and elastic recovery [1,22]. Consistent with this, a recent optimization study for Ti–6Al–4V identified feed as the most influential factor for burr minimization across both up and down-milling strategies [23]. Process-window studies showed that balanced combinations of feed rate and cutting speed (V_c) minimize burr formation, whereas progressive wear correlates with larger top and lateral burrs and degraded surface finish [24].

Cutting speed acts through temperature, chip segmentation, and the length of the chip–workpiece contact. Raising speed increases interface temperature and promotes thermal softening. When shearing is facilitated, the contact shortens and burr width decreases [12]. At very small feeds dominated by rubbing, an adhesive transfer layer and built-up edge (BUE) can develop and the cutting speed benefit diminishes [25]. Parameter optimization further indicates depth of cut mainly affects burr height, whereas feed and speed are more influential for surface roughness and burr width [9,13]. Finite-element classification showed that reducing the ratio of axial depth of cut to edge radius and maintaining sharpness curtailed top burr size, and that slot base burrs are characteristic of micro ball-end milling [13]. Additional work reported that burr height depends strongly on sharpness and chip thickness; even with very sharp tools, a residual burr forms when chip thickness is extremely small [26]. Geometry interacts with these levers: as slot aspect ratio increases, chip evacuation is restricted and both top and sidewall burrs grow [27]. In Ti–6Al–4V, pre-stressing by ultrasonic cavitation peening reduced burr width and height by about two-thirds by restricting lateral flow [28].

1.2. Milling strategies

Milling strategy determines where the instantaneous chip thickness approaches zero and therefore which burr mode dominates. Under commonly used conditions, up-milling produces rougher surfaces with more pronounced burrs, whereas down-milling gives smoother surfaces with smaller burrs [29]. Strategy interacts with parameters: in one study, reducing feed improved surface finish by stabilizing chip flow, but it also led to more burr formation. Within that low-feed window, up-milling produced smaller burrs, while down-milling produced larger, wavy burrs [30]. Tooling also matters: adding flutes reduced burr height in both strategies, and tool diameter and depth of cut strongly influenced burr height and thickness in that setup [31]. Side differences in Ti–6Al–4V arise from distinct mechanisms. In up-milling the top edge burr is driven mainly by edge radius extrusion, while in down-milling it results from extrusion together with chip turnover and tearing. On the other hand, raising feed stabilizes shearing and narrows the burr on both sides [25].

Cutting speed and tool wear shift the balance of mechanisms. When speed enters the ultra-high regime, segmented chips form in a regular pattern. That regularity shortens chip–tool contact at the up-milling exit and reduces the resulting edge burr [32]. As the edge rounds with wear, top burr height increases, especially in down-milling, through changes in chip-formation angles and force components [33]. In down-milling, response-surface optimization identified spindle speed and feed as the primary drivers of burr width. The optimum lay at low feed and low depth of cut, which reduced exit-side thrust and limited edge radius extrusion [34]. Assistance strategies act by reducing ploughing and shaping the force waveform. Vibration-assisted micro-milling decreased burr formation, particularly on the down-milling side, by reducing ploughing effects and modulating cutting dynamics [35]. In Ti–6Al–4V, longitudinal torsional ultrasonic assistance promoted chip breakage, lowered forces and temperature, and produced smaller burrs at the same nominal feed and speed [36]. High-speed tests also reported larger top burrs in up-milling at elevated cutting speed and smaller burrs in down-milling at conventional speed, underscoring the speed strategy interaction [37].

1.3. Lubrication strategies

Cooling and lubrication set the tribological and thermal state at the tool–chip contact and, in turn, shape wear and edge formation. In micro-milling Ti–6Al–4V, MQL improved tool life, reduced wear, and lowered roughness relative to dry cutting. Higher air pressure, however, enlarged the edge lip, showing that delivery conditions matter [38]. Directing the MQL jet along the feed reduced both burr formation and tool wear compared with dry cutting [39]. Although MQL often helps, one study reported longer tool life in dry cutting due to a stabilized BUE, despite MQL giving better surface quality [40]. Delivery rate is also important at small scales: in Ti–6Al–4V micro-drilling, a low MQL flow near 6 mL per hour reduced thrust, specific cutting energy, and hole roughness more effectively than higher flows, consistent with better penetration of the interface [41].

Hybrid routes strengthen cooling while preserving boundary lubrication. Combining MQL with chilled air produced the lowest wear and smallest edge lip in micro-milling, whereas chilled air alone increased chipping and raised burr formation [42]. When nanofluid MQL mixed with cold CO_2, a low particle fraction improved penetration and heat removal, lowering forces and wear; a higher fraction strengthened boundary lubrication and improved surface finish [43]. For additively manufactured Ti–6Al–4V, MQL extended tool life and improved surface finish, but increased burr size when compared with dry cutting. Burr size increased with feed rate, and higher cutting speed reduced burr height under both conditions [44]. At higher thermal loads, supercritical CO_2 combined with MQL has performed well in titanium milling. When compared with emulsion flood, $scCO_2$+MQL reduced tool wear and improved throughput in high-speed milling of Ti–6Al–4V [45].

1.4. Research gap and objectives

Literature underscores the various factors that contribute to burr formation during the micro-milling of titanium alloys, particularly Ti–6Al–4V. The joint influence of feed per tooth, cutting speed, axial depth of cut, and cooling strategies across the different cutting speed ranges on both burr width and height in up and down-milling of Ti–6Al–4V has not been mapped systematically. Fig. 1 shows there are three distinct cutting speed ranges that are recognized for titanium and its alloys: conventional-speed machining (CSM) (V_c = 10–50 m/min), transition-speed machining (TSM) (V_c = 50–102 m/min), and high-speed machining (HSM) (V_c = 102–1000 m/min) [17]. This study (1) measures burr width and height across CSM, TSM, and HSM using an L9 design that varies f_z, V_c, a_p and cooling condition (dry, MQL, wet); (2) quantifies factor effects and significance with main effects plots and ANOVA; (3) explains trends using a mechanism-based framework; and

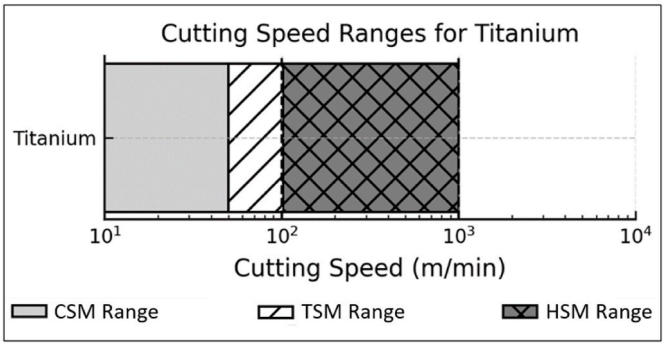

Fig. 1. Cutting speed ranges for Titanium.

(4) validates the optimal set of parameters experimentally.

2. Material and methods

Fig. 2 summarizes the workflow of the study, from selection of material to validation (optimum check).

2.1. Workpiece material

The selected material for the experiments was grade 5 titanium alloy, Ti–6Al–4V. This material consists of both alpha (α) and beta (β) phases, with the α phase making up approximately 60–90 % and the β phase comprising 10–40 % at room temperature. The α phase, characterized by a hexagonal close-packed (HCP) structure, remains stable from room temperature onward, whereas the β phase, which has a body-centered cubic (BCC) structure, remains stable up to the alloy's melting point. The stability of these phases is influenced by specific alloying elements [19]. Alpha stabilizers such as nitrogen, carbon, aluminum and oxygen enhance the stability of the α phase, while beta stabilizers like vanadium, molybdenum, manganese, chromium, and iron promote β phase stability [46,47]. The mechanical properties, physical properties and chemical composition are provided in Tables S1–S3, respectively.

2.2. Experimental setup

Micro-milling experiments were conducted on a Yida MV-1060 CNC milling center under dry, minimum quantity lubrication (MQL), and wet cooling conditions, as illustrated in Fig. 3. The machine's internal system supplied Shell Dromus B; wet flow was 6 L/min, and MQL was 40 mL/h, based on recommendations from the literature [48]. To achieve high-speed milling, the NAKANISHI HES810-BT40 attachment, capable of reaching a maximum speed of 80,000 rpm, was utilized. Precise Z-axis measurements were achieved using a BMD 410V tool pre-setter. Burr measurements were taken on an Olympus DSX1000 digital microscope. The field of view was 667 × 667 μm at 1200 × 1200 pixels. The system's guaranteed measurement performance was XY magnification accuracy 3 % (after calibration), XY repeatability ±2 % (3σ), and Z-axis height repeatability ≤1 μm with ≥20 × objectives. Each experiment was conducted twice to assess error variance. For every trial, the maximum burr width and height were recorded, and the average values from both runs were used for subsequent analysis. Experimental conditions are listed in Table 1.

2.3. Cutting tool specifications

To level the workpiece surface, a carbide end mill was utilized, with the finished surface serving as the reference for micro-milling experiments. The measured average edge radius of the micro tools was 3.5 ± 0.5 μm. Full specifications are provided in Table 2.

2.4. Design of experiment

An L9 Taguchi array was used with four factors at three levels: f_z, V_c, a_p, and cooling condition. Prior research has shown that when the feed rate is lower than the tool's edge radius, residual effects become more pronounced [1]. To mitigate these effects, the feed per tooth was selected above the tool's edge radius. The range of a_p for tool was determined based on its diameter, with specific recommended values to ensure optimal machining performance. As per literature [14] for tools with a diameter of 3.18 mm or smaller, the corresponding a_p values have been provided in Table 3.

The feed speed (V_f) and spindle speed (N) can be determined using the following equations, which define their relationship with key machining parameters [1].

$$V_f = f_z \times N \times z \ (\text{mm} / \text{min}) \tag{1}$$

$$N = \frac{V_c}{\pi \times D} \ (\text{rpm}) \tag{2}$$

Since the high-speed milling attachment was controlled in rpm, the three speed levels within each cutting speed range were selected in rpm and then converted to V_c. The details of the process parameters and their corresponding levels are given in Table 4.

3. Results

During the micro-milling process, various types of burrs can develop depending on the cutting direction and the interaction between the tool and workpiece. These include top burr, bottom burr, entrance burr, side burr and exit burr. The exit burr and side burr are found on the surfaces machined by the tool's minor and major cutting edges, respectively [30]. The top burr remains on the top surface of the workpiece [14]. During the micro-milling process, chips generated by the cutting tool move upward along its rake face, creating significant tensile stress that pulls apart the material in contact with the chips and workpiece. Part of this deformed material adheres to the top surface instead of being carried away with the chips, leading to the formation of top burrs [13]. Fig. 4 shows how the top burr width and height were measured [14].

3.1. Burr measurement

Fig. 5 illustrates the rotation of the micro tool, the feed direction, and the formation of burrs on both the down-milling and up-milling sides of the machined slot during micro-milling. For each run, the maximum

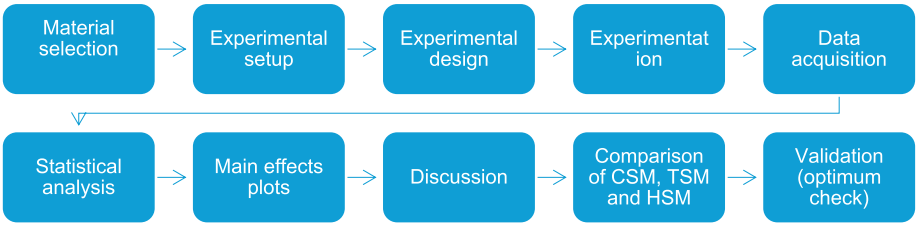

Fig. 2. Workflow of the study.

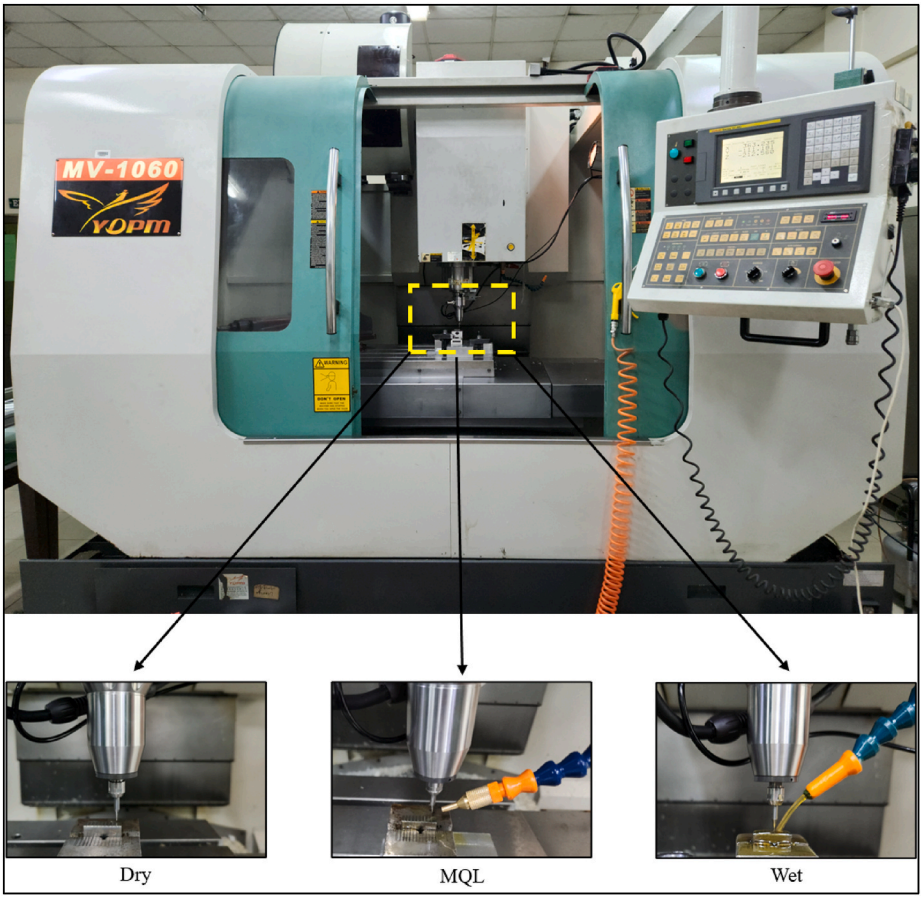

Fig. 3. Experimental setup illustrating machining under dry, MQL and wet cooling conditions.

Table 1
Experimental conditions.

Parameter	Specification
Milling type	Full immersion
Cooling condition	Dry, MQL, Wet
Workpiece Dimensions (L × W × H)	10 mm × 20 mm × 50 mm
Cutting Length	10 mm

Table 2
Cutting tool specifications.

Item	Description
Brand	North Carbide Tools
Material	Tungsten Carbide
Type	End Mill
Overall length	50 mm
Helix angle	60°
Tool diameter (D)	0.5 mm
Blade length	1 mm
Number of flutes (z)	2

Table 3
Values of axial depth of cut.

Description	Formula	Value
Recommended a_p	D × (0.05–0.25)	–
Minimum a_p	0.5 × 0.05	25 μm
Maximum a_p	0.5 × 0.25	125 μm

burr width and height of the top burr were measured for both up-milling and down-milling operations using an Olympus DSX1000 digital microscope. Fig. 6 shows the measurement of top burr width, while Fig. 7(a and b) illustrates the burr height measurement in both 2D and 3D views using the digital microscope. The mean ± standard deviation (SD) bar charts by factor level are provided in the Supplementary Material: CSM (Figs. S1–S4), TSM (Figs. S5–S8), and HSM (Figs. S9–S12). Each figure contains four panels (feed per tooth, cutting speed, depth of cut, and cooling condition) and reports up and down-milling responses separately. Tables S4–S6 report the Taguchi L9 datasets for CSM, TSM, and HSM. Figs. S13–S15 present representative DSX1000 micrographs of machined slots, illustrating the measurement of top burr width and height on both sides (up and down-milling) across all cutting speed ranges.

3.2. Application of ANOVA

Following the measurement of top burr width and height using a microscope, statistical analysis was performed using the Analysis of Variance (ANOVA) technique in Minitab software. ANOVA is a widely used statistical method that assesses the significance of process parameters in influencing output responses, providing a quantitative understanding of their impact on outputs. The analysis involved calculating the sequential sum of squares (SS_A) for each parameter using the following equation [49].

$$SS_A = \sum_{i=1}^{3} \frac{A_i^2}{n} - \frac{\left(\sum_{j=1}^{N} T_j\right)^2}{N} \tag{3}$$

The process parameter is denoted by A, while n represents the total

Table 4
Machining parameters, their levels and values.

Process Parameter	f_z (μm/tooth)	V_c (m/min)			a_p (μm)	Cooling Condition
		Conventional	Transition	High-speed		
Level 1	8	25.135	64.407	103.680	50	Dry
Level 2	10	36.131	75.404	114.676	75	MQL
Level 3	12	47.127	86.400	125.673	100	Wet

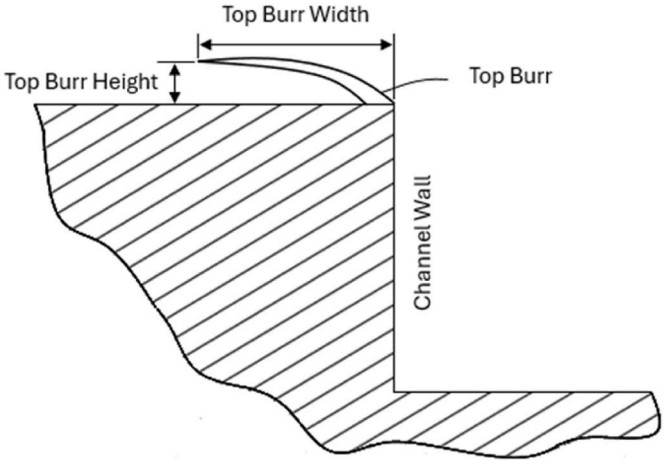

Fig. 4. Top burr width and height measurement [14].

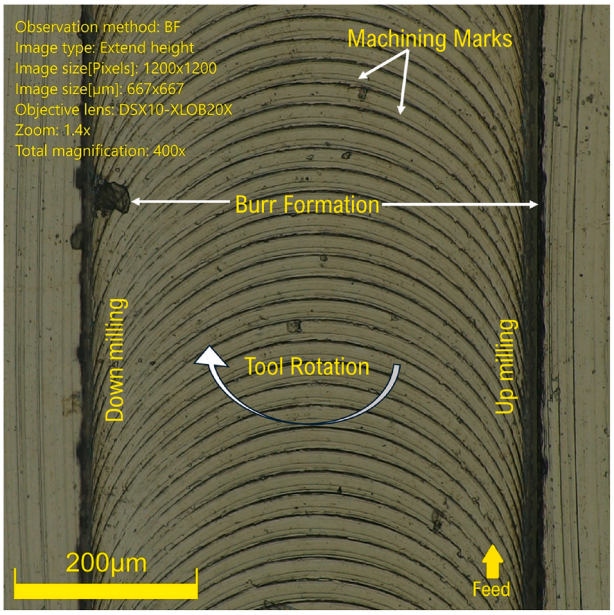

Fig. 5. Magnified view of machined slot highlighting surface characteristics.

number of runs at a given level. The variable I refers to the level, and T corresponds to the response value recorded for each run, where j is the specific run number, and N indicates the overall number of runs. The total sum of squares (SS_T) was calculated using the corresponding equation [49].

$$SS_T = \sum_{j=1}^{N} T_j^2 - \frac{\left(\sum_{j=1}^{N} T_j\right)^2}{N} \tag{4}$$

The sequential sum of squares for error (SS_e) was subsequently

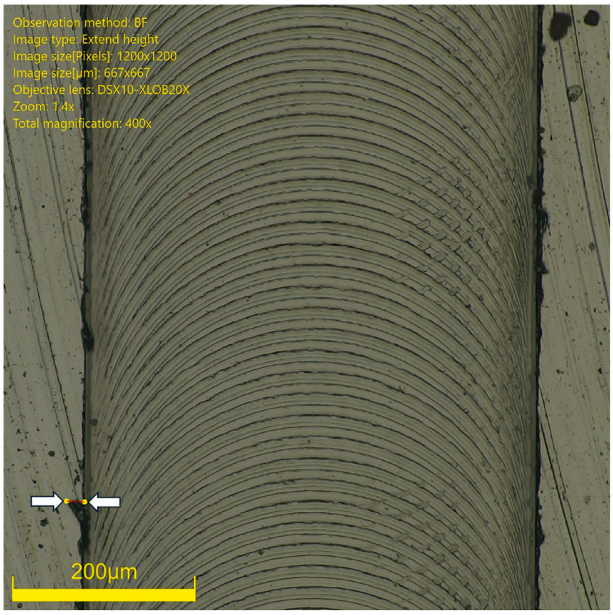

Fig. 6. Burr width measurement – down-milling side.

calculated using the following equation [49]. Z represents the total number of factors considered in the analysis.

$$SS_e = SS_T - \sum_{i=A}^{Z} SS_i \tag{5}$$

The F-test ratio for each parameter was analyzed, where a smaller F-value indicates a minimal impact of that parameter on the outcome, while a larger value signifies a higher impact. Additionally, the p-value, which quantifies the probability of a test failing, was utilized to evaluate statistical significance. A p-value below 0.05 (5 %) indicates a 5 % probability of failure and a 95 % probability of success. The percentage of contribution ratio (CR) of each parameter to the total variance was determined using the following equation [49]. DoF represents the degrees of freedom and MSS_{Res} represents the mean sum of squares for residuals.

$$\%CR = \frac{SS - (DoF \text{ x } MSS_{Res})}{SS_T} \text{ x } 100 \tag{6}$$

Figs. 8–10 present the contribution ratio and statistical significance of the machining parameters, as obtained from the ANOVA analysis, for burr width and height on the up and down-milling sides under conventional, transition, and high-speed cutting ranges, respectively. For comprehensive ANOVA analysis, see Tables S7–S10 (CSM), S11–S14 (TSM), S15–S18 (HSM).

4. Discussion and analysis

4.1. Conventional-speed

4.1.1. Burr width (up-milling and down-milling)

Fig. 8 indicates that f_z is the most significant factor influencing burr

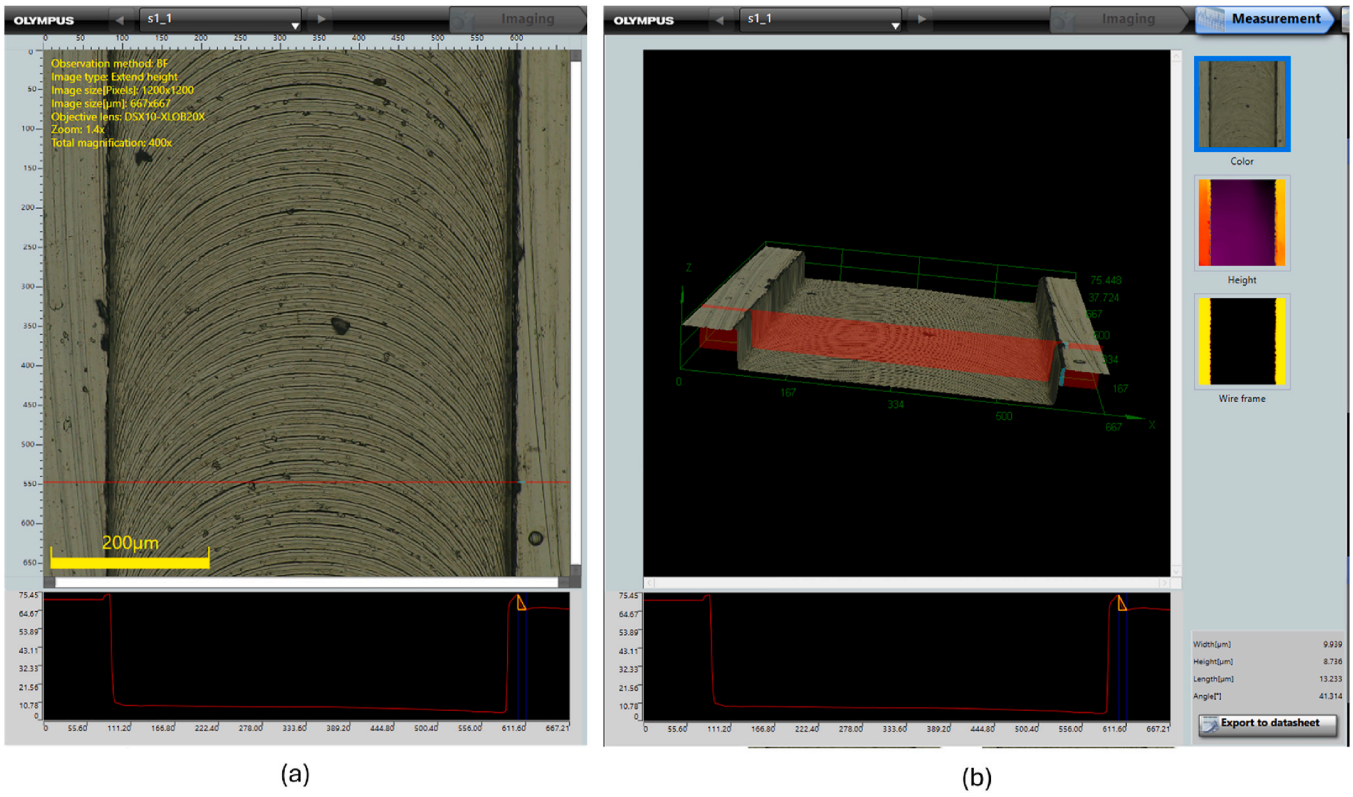

Fig. 7. Burr height measurement – up-milling side (a) 2D view; (b) 3D view.

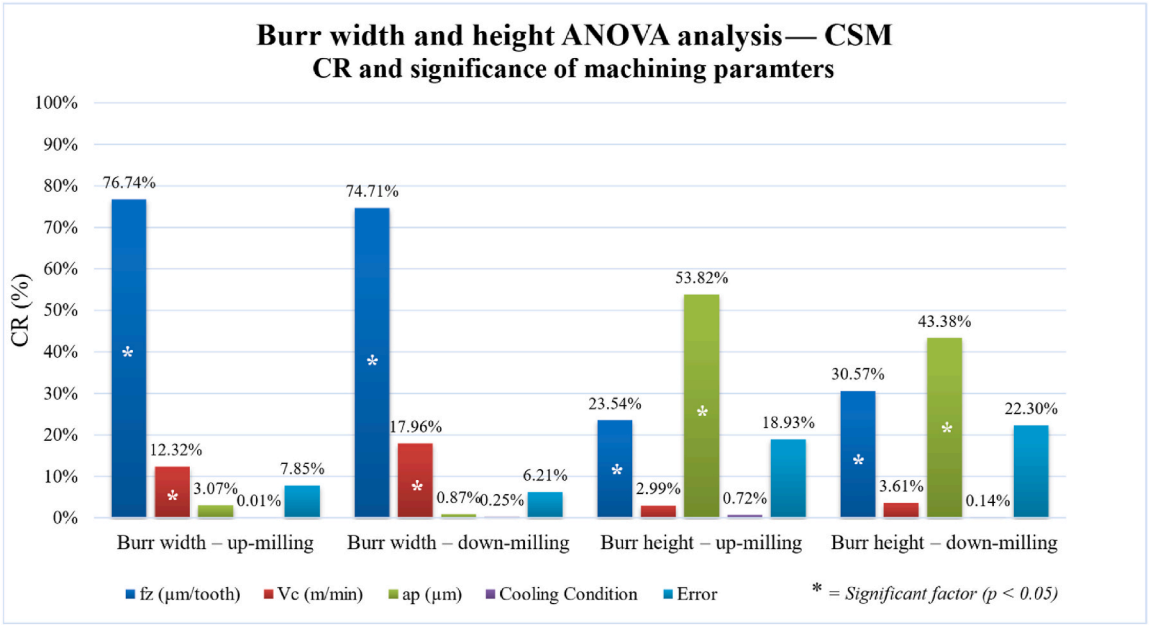

Fig. 8. CR and significance of machining parameters for burr width and height – ANOVA analysis (CSM).

formation in both up-milling and down-milling operations. In up-milling and down-milling, f_z exhibits a very high CR of 76.74 % and 74.71 %, respectively, highlighting its dominant role in burr width variation. In both milling configurations, V_c is the second most significant factor, with a CR of 12.32 % in up-milling and 17.96 % in down-milling. a_p and cooling conditions appear to have negligible influence in both milling configurations.

From the main effects plots (Fig. 11), a clear pattern is observed: as feed per tooth increases, burr width consistently decreases in both up and down-milling. Researchers have reported similar outcomes and found that at lower feed rates, chip thickness approaches or falls below the cutting-edge radius, leading to rubbing and ploughing actions rather than efficient shearing [14]. This inefficient cutting condition promotes lateral material flow and burr formation. Increasing feed rate shifts the cutting mechanics toward a more stable shearing regime which reduces lateral material displacement and minimizes burr width [18].

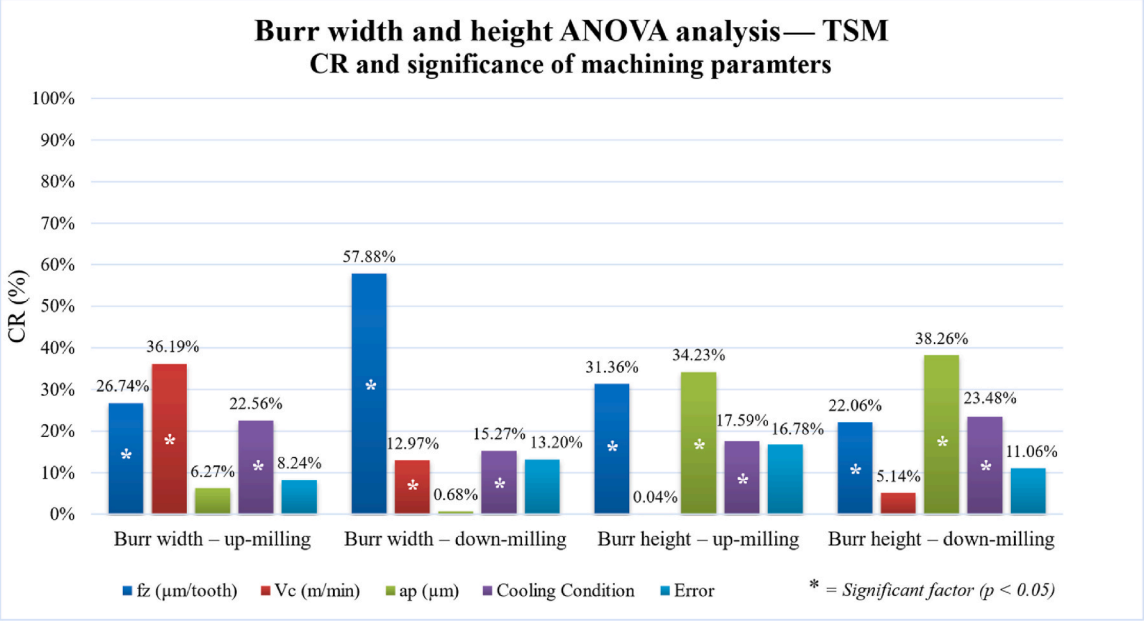

Fig. 9. CR and significance of machining parameters for burr width and height – ANOVA analysis (TSM).

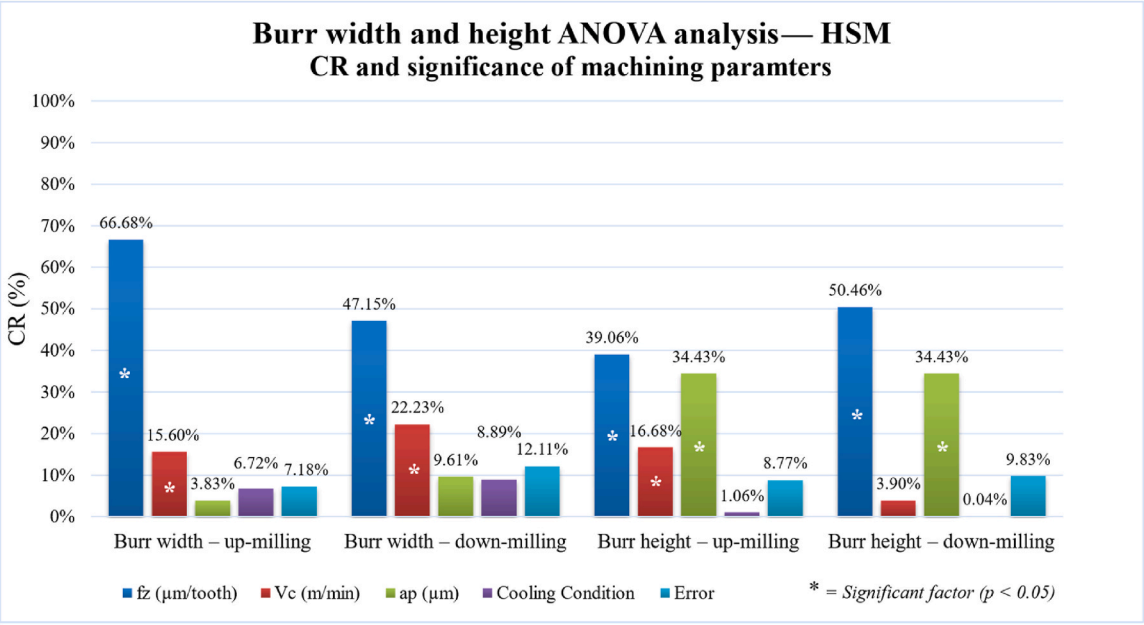

Fig. 10. CR and significance of machining parameters for burr width and height – ANOVA analysis (HSM).

Cutting speed affects burr width. Burr width decreases as V_c increases. In Ti–6Al–4V, this can be explained by thermal softening dominating over rate-dependent hardening in the primary and secondary shear zones. As V_c rises, local temperature increases and the flow stress drops; it produces segmented-shear chips more readily, the chip–workpiece attachment length shortens, and lateral side-flow is reduced, which altogether reduces burr width [25,50,51]. Related observations on speed-dependent heat input and softening-controlled plastic flow have been reported in friction-based solid-state deposition studies [52]. Similar process-structure-property mapping has been shown for modified friction stir deposition where higher rotational speed increases heat, enhances plastic flow, and alters near-surface geometry [53]. This analogy is consistent with AFSD heat-input formulations and observations (e.g., Q increasing with rotational speed and feed) and the degradation of layer quality under excessive heat input [54,55].

Although the depth of cut is not statistically significant for burr width (CR 3.07 % in up-milling and 0.86 % in down-milling), the up-milling side shows a consistent decrease in burr width with increasing a_p. The mechanism can be attributed to heat partitioning effect: larger a_p increases the uncut chip thickness and chip volume per tooth, so a greater share of shear heat is carried away by the outgoing chip rather than conducted into the workpiece. The reduced subsurface thermal load lowers lateral side flow at the tool exit and shortens the chip–workpiece attachment length, which reduces burr width [56,57]. In contrast, down-milling produces a chip that thins to nearly zero at exit; burrs initiate where the instantaneous chip thickness is small and ploughing/bending dominate, which makes the effect of a_p on burr width weak

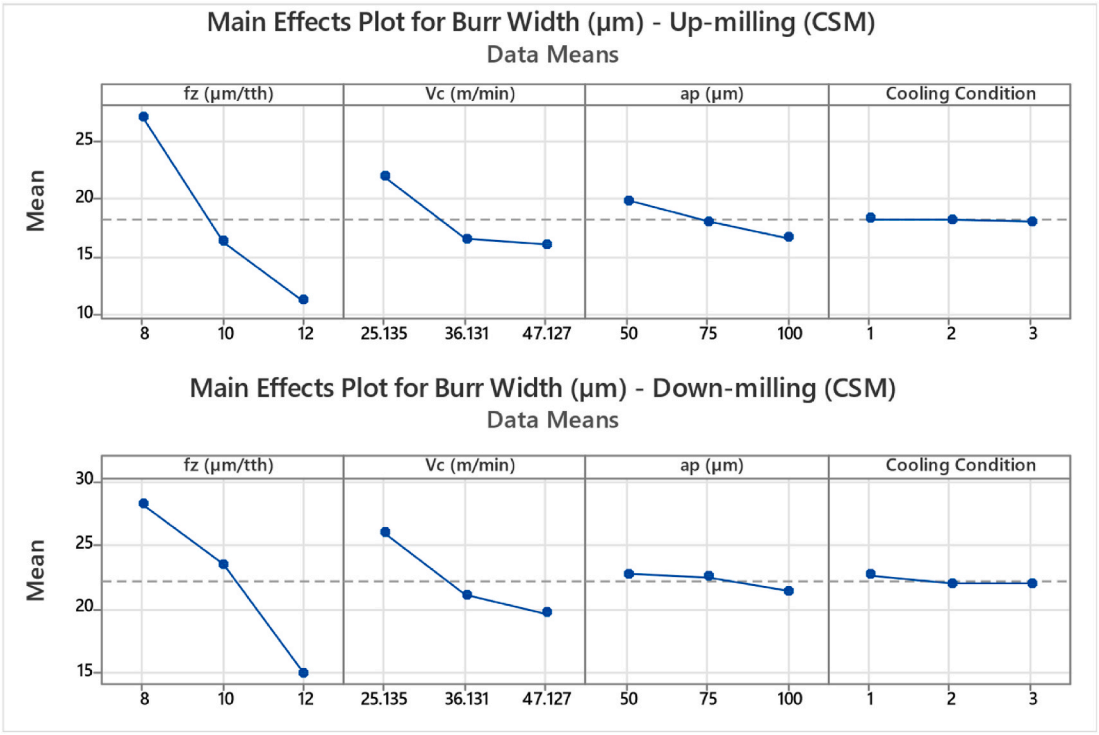

Fig. 11. Main effects plot illustrating the influence of process parameters on burr width (µm) – up-milling and down-milling (CSM).

or absent [25,27,28].

The cooling conditions show no statistical significance and low CR of 0.01 % in up-milling and 0.25 % in down-milling for burr width. The main effects lines are shallow, and the wet condition lies slightly lower. Therefore, cooling comes as a secondary factor for burr width in CSM, with f_z and V_c dominating the response. Similar observations have been reported for Ti–6Al–4V micro-machining, where lubrication improves tribology and tool behavior, but burr formation is mainly governed by chip-thickness kinematics and thermal input from speed [44,58].

4.1.2. *Burr height (up-milling and down-milling)*

Fig. 8 shows that a_p and f_z are significant for burr height in both milling directions, with a_p as the most influential factor. In contrast, V_c and cooling conditions do not show any statistical significance in both

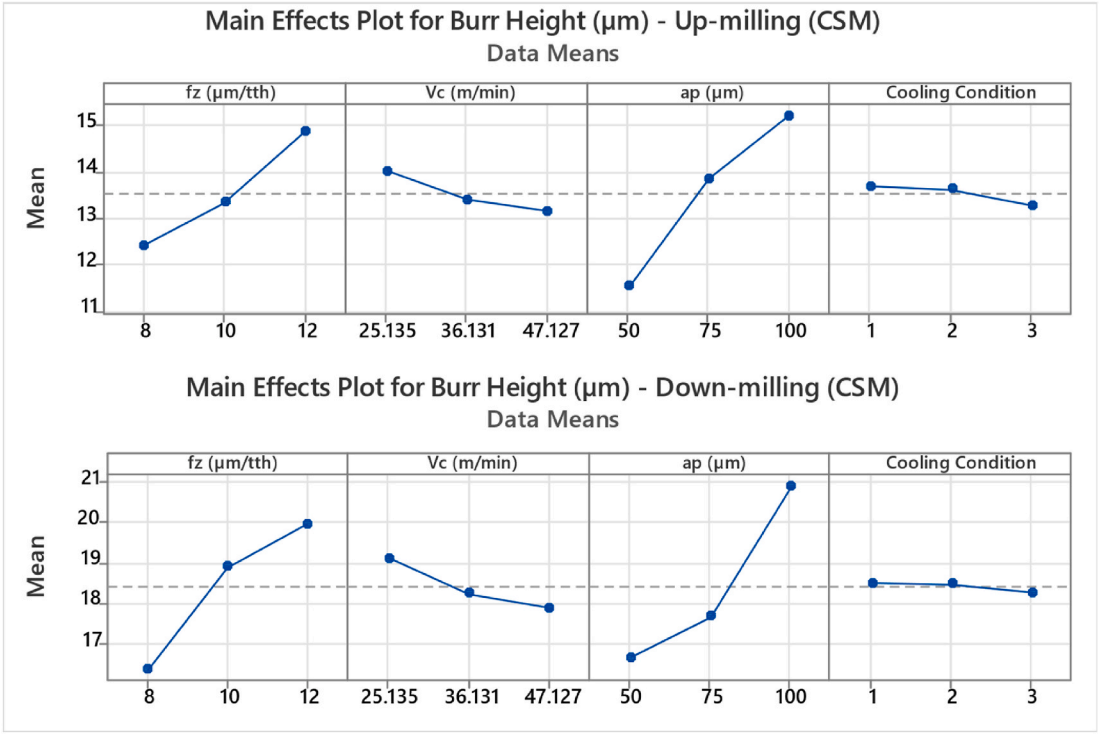

Fig. 12. Main effects plot illustrating the influence of process parameters on burr height (µm) – up-milling and down-milling (CSM).

the cases. Increasing a_p and f_z raises the instantaneous uncut chip thickness and the engaged contact length. The larger engagement increases thrust and normal stress at the tool exit, expands the secondary deformation zone, and increases the local compressive to shear force ratio. The free edge of the remaining ligament bends more before separation and more material is extruded onto the top surface, so burr height increases. This behavior is consistent with recent experiments and finite-element analyses which link exit-side bending and extrusion to the burr height [25,27,28,33].

Cutting speed is not statistically significant for burr height in CSM (CR 2.99 % in up-milling; 3.61 % in down-milling; Fig. 8). The main effects plots (Fig. 12) show a slight decrease with increasing V_c, which is consistent with thermal softening at higher speed, but this effect is small when compared with engagement controlled increase in thrust and exit-side bending from a_p and f_z which makes it non-significant [25,50,51]. Cooling condition is also non-significant for burr height in CSM (up-milling CR 0.72 %; down-milling CR 0.14 %; Fig. 8). Its directional behavior mirrors the CSM burr width case. It has slight physical effect on burr formation in CSM but carries no significance when compared to a_p and f_z for burr height.

4.2. Transition-speed

4.2.1. Burr width (up-milling and down-milling)

From Fig. 9 it can be observed that f_z, V_c and cooling condition are significant for burr width, whereas a_p is non-significant in both milling directions. The main effects plots (Fig. 13) for TSM show a similar trend for f_z and a_p as in CSM where increasing feed rate and depth of cut decreases the burr width. For the V_c and cooling condition the trend differs from CSM. For cutting speed, burr width first decreases from 64.407 to 75.404 m/min and then increases from 75.404 to 86.400 m/min (Fig. 13). The initial decrease is consistent with thermal softening that favors cleaner shearing in this range [25]. At higher speeds, titanium's high adhesion promotes a transfer layer and transient BUE that behaves as a virtual cutting edge and increases the effective edge radius [50]. The larger effective radius increases the minimum chip thickness and shifts the exit contact towards ploughing, which lengthens the attachment and increases lateral extrusion on the top surface [33,50]. Segmented chip formation intensifies, and intermittent loss of the transfer layer leaves uncut ligaments, which increase burr width [25,58]. Similar findings have been reported by Baig et al. [59] noting that burr width tends to increase in both types of milling operations as the cutting speed rises from 75 m/min to 100 m/min.

CR of cooling condition has increased in TSM compared to CSM, making it a significant factor. For both up and down-milling, results show that MQL cooling condition has reduced the burr width. At higher cutting speeds, the thermal and mechanical conditions in the micro-milling of Ti–6Al–4V significantly influence burr formation due to increased heat generation at the tool-workpiece interface. While wet cooling has traditionally been used to dissipate heat, its efficiency diminishes as the cutting temperature rises rapidly in the transition speed range. This is mainly due to the boiling and vaporization of the coolant, which disrupts the continuous cooling film and reduces its heat transfer capability [60]. Moreover, the bulk fluid flow in wet conditions struggles to penetrate the confined tool-chip interface effectively in micro-milling operations. In contrast, MQL provides a fine mist of lubricant that penetrates these micro-gaps more efficiently. The rapid evaporation of the oil mist removes heat through latent heat absorption, a mechanism that becomes more effective than wet cooling under high cutting speeds [58]. The improved chip evacuation facilitated by MQL also prevents chip recirculation and redeposition, which are common contributors to burr formation under wet conditions. Therefore, MQL demonstrates superior performance in controlling burr formation (burr width and burr height) in the transition speed range by effectively balancing localized lubrication and heat dissipation.

4.2.2. Burr height (up-milling and down-milling)

During TSM, Fig. 9 for burr height (up-milling and down-milling) shows that f_z, a_p and cooling condition are the significant factors affecting the burr height. V_c is non-significant for burr height in both up and down-milling because height is controlled by exit-side bending and extrusion of the remaining ligament, which are mainly determined by

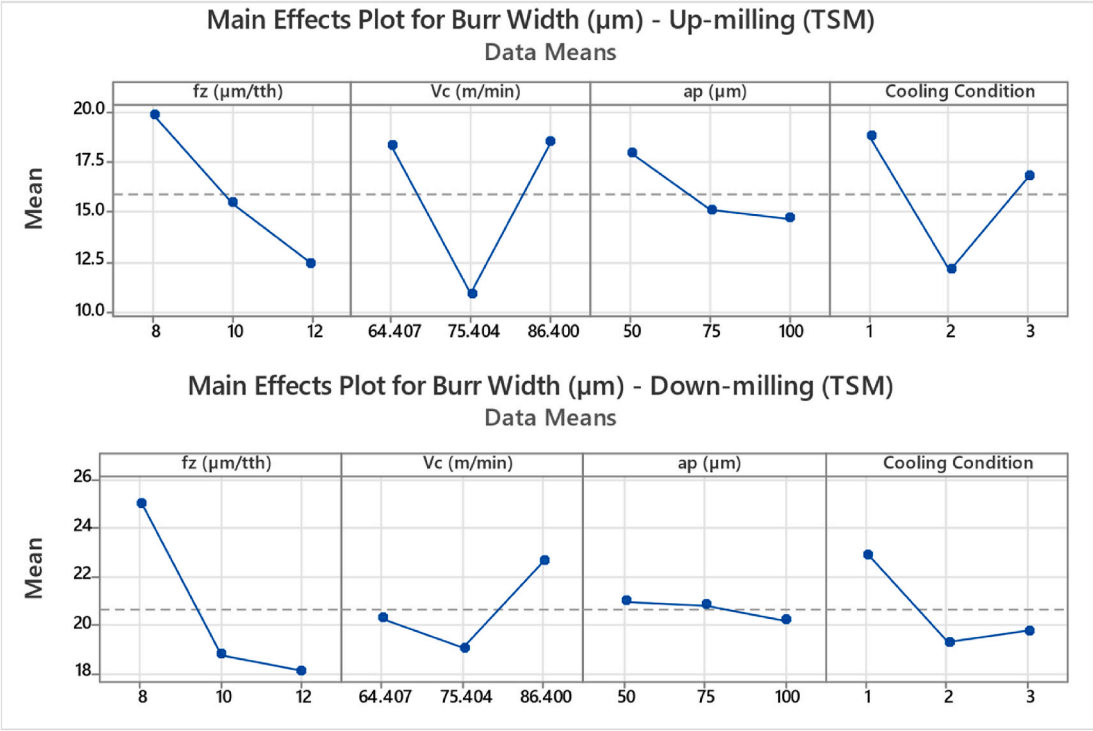

Fig. 13. Main effects plot illustrating the influence of process parameters on burr width (µm) – up-milling and down-milling (TSM).

engagement and thrust from a_p and f_z [28,33]. In contrast, burr width is sensitive to temperature and adhesion-driven changes in chip–workpiece attachment and lateral flow, which explains the significance and influence of V_c on burr width but not on height [25,50,51]. The depth of cut has been identified as the most significant factor affecting burr height in both up-milling and down-milling. The main effects plots (Fig. 14) for f_z and a_p indicate a clear trend: burr height increases as both parameters rise. Similar trends were observed for burr height (up-milling and down-milling) in CSM and explained in detail. The main effects plots (Fig. 14) for burr height (both milling directions) show similar trend as for burr width in transition speed range with V_c of 75.404 m/min and cooling condition of MQL showing minimum burr formation (burr width and height).

4.3. High-speed

4.3.1. Burr width (up-milling and down-milling)

Burr width measurements under HSM indicate that feed per tooth was the most critical factor affecting burr width in both up-milling and down-milling. From Fig. 10, it is evident that f_z contributed the largest share (66.68 %) to the total variation in burr width during up-milling, followed by V_c at 15.6 %. Similar trends were observed in down-milling, where f_z accounted for 47.15 % of the total contribution ratio and V_c for 22.23 %. Although both depth of cut and cooling condition showed visible trends in the main effects plots (Fig. 15) for up-milling and down-milling, their statistical significance levels indicate that these factors are not significant for burr width under HSM conditions.

The observed trends of burr width against f_z, V_c, a_p and cooling condition are similar to that of CSM for up-milling and down-milling strategies. Baig et al. [59] have reported in their research that an increase in cutting speed from 100 m/min to 125 m/min results in a reduction in burr width, further corroborating the current results.

4.3.2. Burr height (up-milling and down-milling)

CR and significance of factors (Fig. 10) under HSM conditions reveal that depth of cut and feed per tooth are the key factors influencing burr height in both milling strategies. In contrast, cutting speed and cooling conditions exhibit either a minimal or statistically insignificant impact. The observed trends (Fig. 16) of burr height against f_z, V_c, a_p and cooling condition are similar to that of CSM. The significance of cutting speed in up-milling and its non-significance in down-milling can be attributed to the distinct mechanics of chip formation in these strategies. Down-milling starts with the maximum chip thickness at the entry, decreasing to zero as the tool exits the workpiece. In up-milling, the tool rotates against the feed direction, the chip thickness starts at zero and increases toward the end of the cut. This “entry rubbing” phenomenon tends to create higher friction and heat at the exit edge, making the process more sensitive to changes in cutting speed [61,62]. As a result, in up-milling, a smaller change in speed can alter the local thermal and mechanical conditions at the tool–workpiece interface which affects burr height.

4.4. Comparison of all 3 speed ranges

Fig. 17 consolidates the factor trends across the three cutting speed ranges and both milling directions. The interaction yields a simple rule: moving below TSM into CSM increases burr width through adhesion-driven lateral flow, whereas moving above TSM to HSM increases burr height via higher thrust and exit-side bending. A single minimum emerges in the TSM range ($V_c \approx 75$ m/min) under MQL, where both burr width and burr height are smallest. The consolidated trends reveal the governing mechanism: increasing f_z curtails lateral flow along the top edge and narrows width, whereas raising a_p and f_z elevates thrust and the exit-side bending moment, increasing height. Within this balance, TSM + MQL provides sufficient lubrication and heat removal to limit adhesion/BUE and shorten contact length, thereby suppressing width without driving the thrust peak that would amplify height.

4.5. Validation experiments

Validation experiments were conducted based on the Taguchi DOE methodology to ensure the reliability of the results. In this study, burr

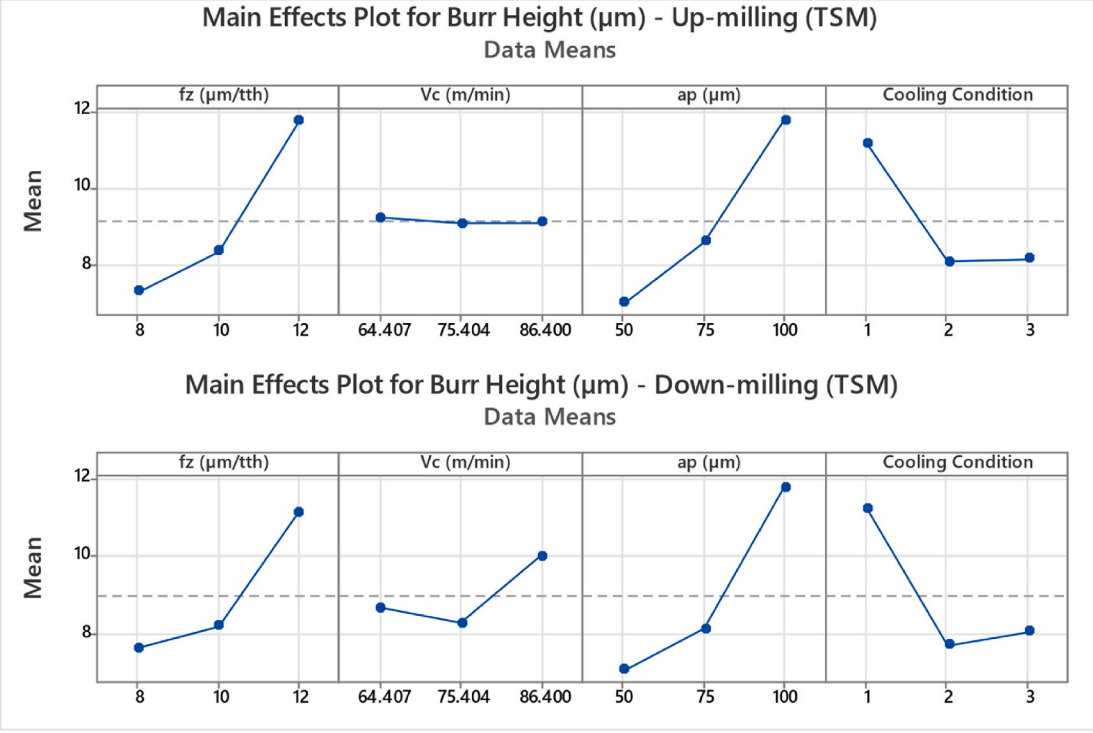

Fig. 14. Main effects plot illustrating the influence of process parameters on burr height (µm) – up-milling and down-milling (TSM).

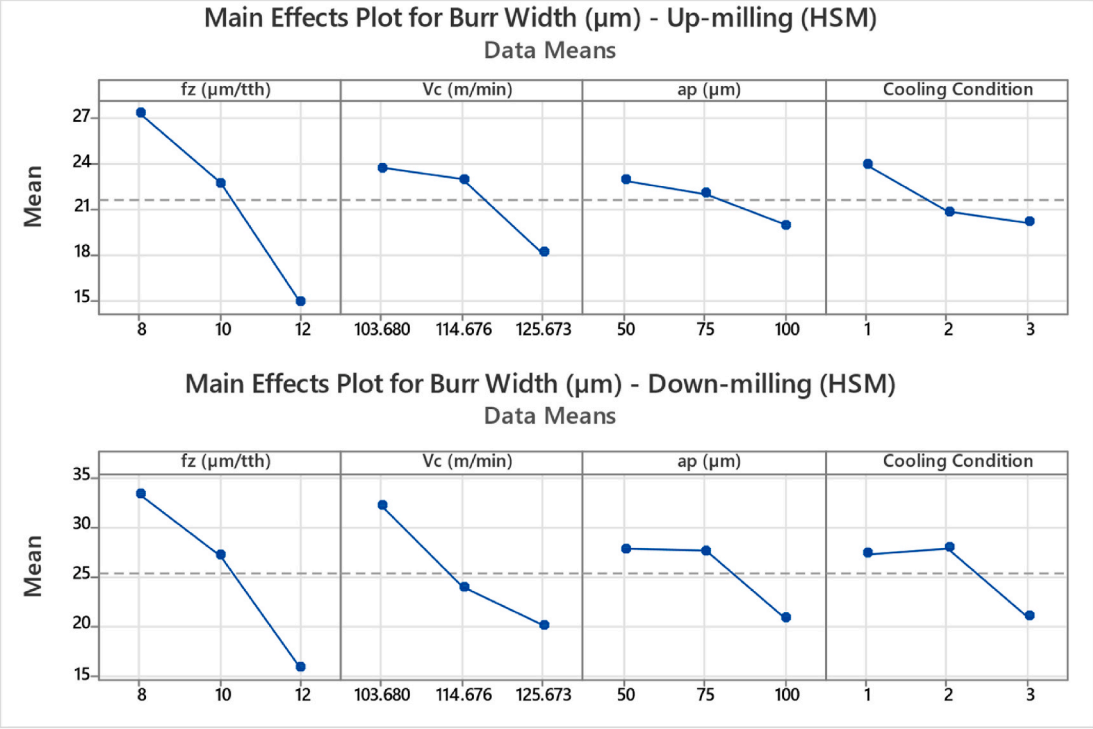

Fig. 15. Main effects plot illustrating the influence of process parameters on burr width (µm) – up-milling and down-milling (HSM).

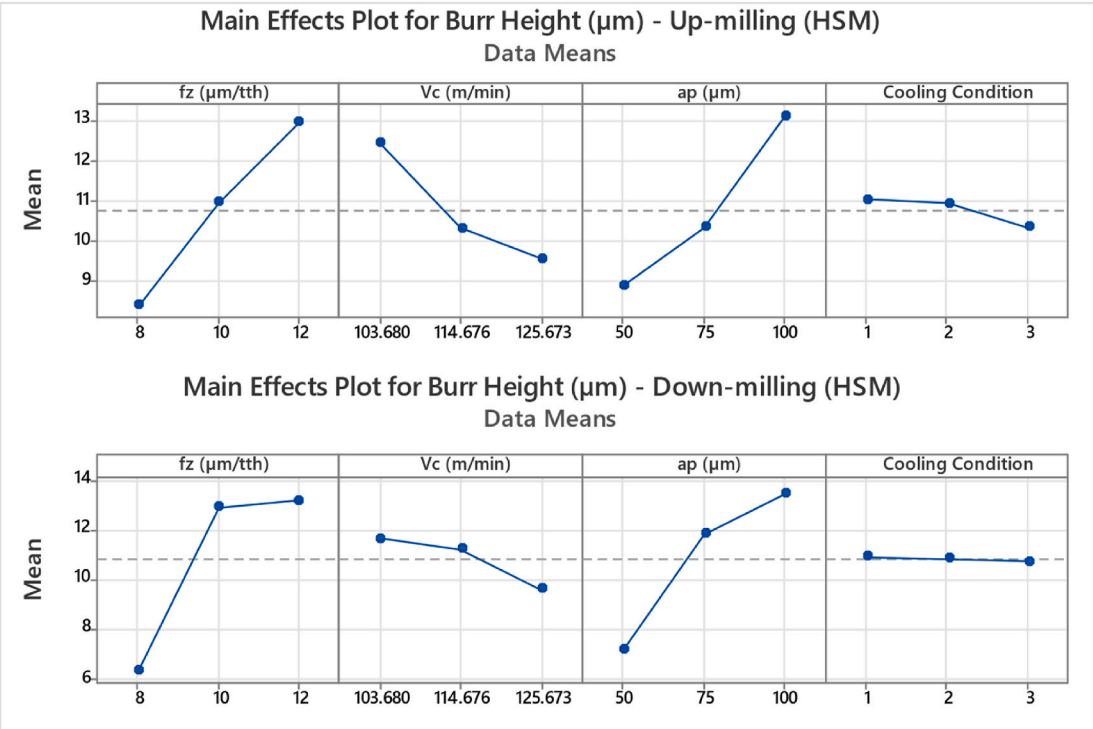

Fig. 16. Main effects plot illustrating the influence of process parameters on burr height (µm) – up-milling and down-milling (HSM).

width and height, evaluated for both milling strategies (up-milling and down-milling), were analyzed using the "smaller is better" optimization approach. Tables 5 and 6 summarize the machining parameter levels that produced the best and worst outcomes for burr width and burr height, respectively. Fig. 18(a and b) presents the optimal results for minimum burr width, while Fig. 19(a and b) presents the optimal results for minimum burr height. These outcomes were obtained using the optimum machining parameters outlined in Table 5.

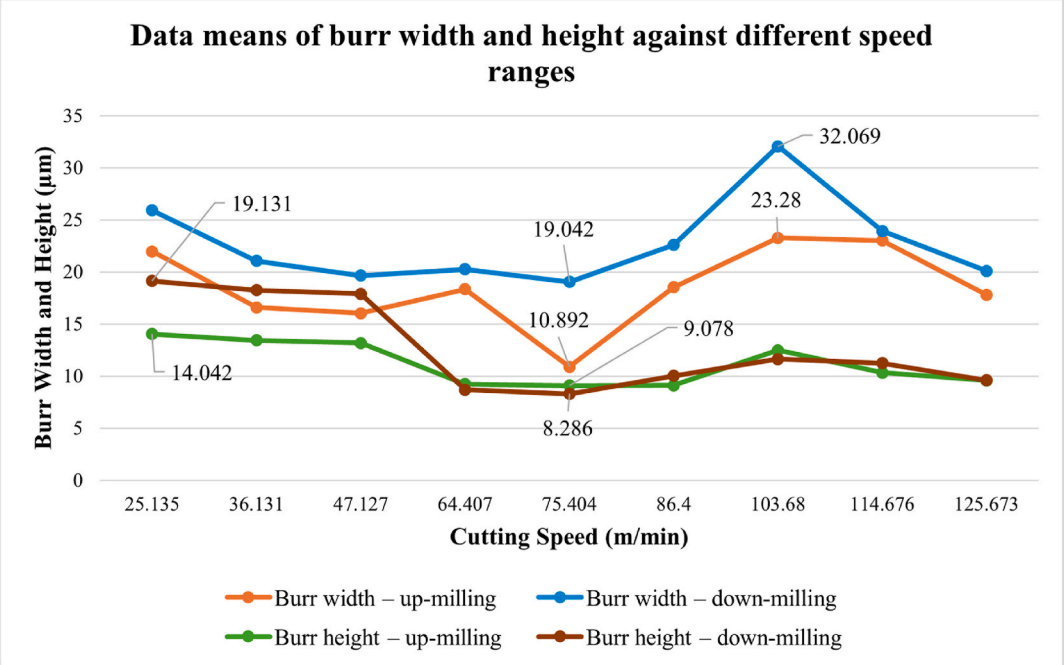

Fig. 17. Mean burr width and height across speed ranges (CSM, TSM, HSM).

Table 5
Validation at optimal conditions.

Test	Output Parameter		f_z (µm/tooth)	V_c (m/min)	a_p (µm)	Cooling Condition	Value (µm)
	Width/height	Milling direction					
1	Burr width	Up	12	75.404	100	MQL	7.257
2	Burr width	Down	12	75.404	100	MQL	11.127
3	Burr height	Up	8	75.404	50	MQL	3.859
4	Burr height	Down	8	75.404	50	MQL	2.730

Table 6
Validation at worst-case conditions.

Test	Output Parameter		f_z (µm/tooth)	V_c (m/min)	a_p (µm)	Cooling Condition	Value (µm)
	Width/height	Milling direction					
1[a]	Burr width	Up	8	103.680	50	Dry	33.047
2[a]	Burr width	Down	8	103.680	50	Dry	44.310
3	Burr height	Up	12	25.135	100	Dry	20.893
4	Burr height	Down	12	25.135	100	Dry	31.25

[a] Tests 1 and 2 were performed during the main experiments.

5. Conclusions and future work

5.1. Conclusions

Identifying key process variables is central to quality and throughput in micro-milling. Using an L9 design with two replicates across conventional, transition and high-speed ranges, four factors were evaluated for their main effects on burr width and height in up and down-milling: feed per tooth, cutting speed, depth of cut and cooling condition. The main conclusions are summarized below.

(1) Across all speed ranges, burr width is governed mainly by feed per tooth and cutting speed, whereas burr height is governed mainly by axial depth of cut and feed per tooth.
(2) The transition-speed range produces the smallest burrs, with a minimum near $V_c \approx 75$ m/min under MQL cooling condition.
(3) In conventional and high-speed ranges, cooling condition has little effect on burr metrics. In transition-speed machining, MQL provides the most favorable lubrication and local heat removal, yielding lower burr width and height.
(4) Increasing f_z generally reduces burr width, whereas higher a_p and f_z increase burr height. Effective control of feed per tooth and depth of cut is critical for reducing burrs in Ti–6Al–4V micro-milling.
(5) Validation experiments at the transition-speed (≈75 m/min) with MQL confirmed the predicted optimum, reducing burr width by 19 % in up-milling, 9 % in down-milling, and lowering burr height by 25 % in both directions, consistent with the mechanisms and factor trends identified in this study.

5.2. Future recommendations

The scope of the present study covers micro-milling experiments on

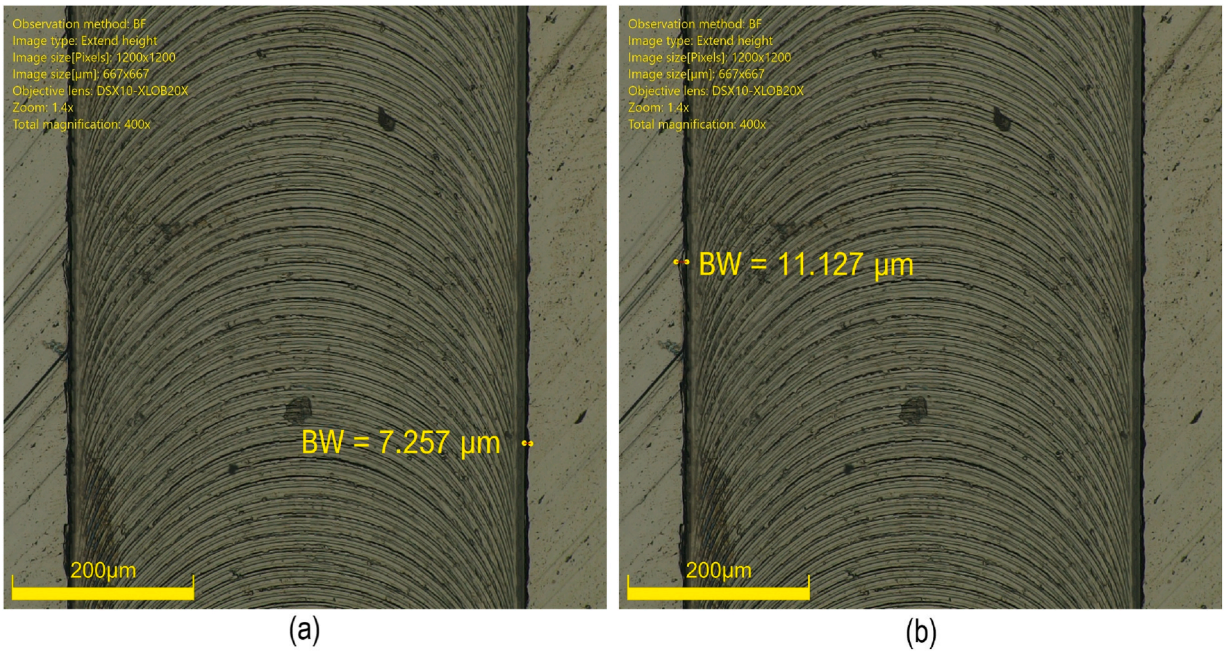

Fig. 18. Minimum burr width (a) up-milling; (b) down-milling.

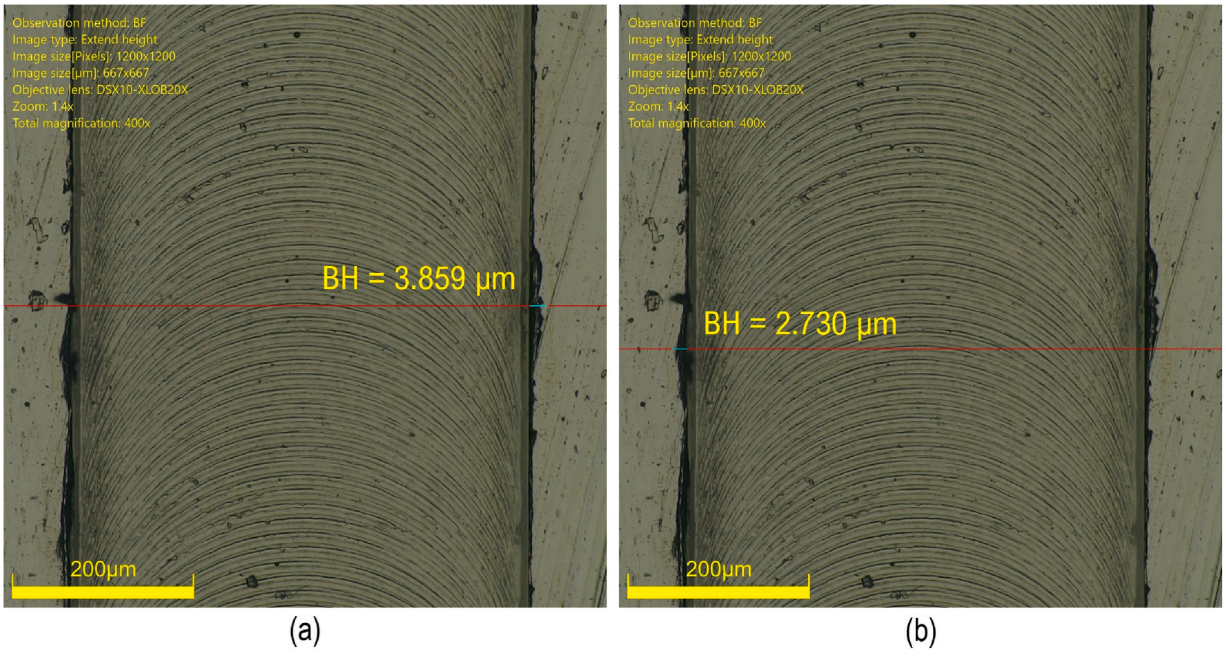

Fig. 19. Minimum burr height (a) up-milling; (b) down-milling.

Ti–6Al–4V, conducted using an L9 Taguchi design with three levels of cutting speed ranges, feed per tooth, axial depth of cut and cooling condition, and evaluated solely in terms of top-edge burr width and height on straight slots. Some future recommendations are: (1) Extend the present study to other titanium alloys and micro-tool geometries including advanced cooling and lubrication strategies to verify and refine the identified burr-formation trends. (2) Compare the current 2D burr metrics with three-dimensional burr morphology, different burr types (entry, side and exit), and detailed subsurface-integrity assessments. (3) Move beyond the L9 design to response-surface and/or Bayesian optimization frameworks that can capture factor interactions and non-linearities in an improved way, using machine-learning models trained on an expanded dataset to refine process windows around the transition-speed regime ($V_c \approx 75$ m/min) under MQL.

Declaration of competing interest

The authors declare that they have no known competing financial interests or personal relationships that could have appeared to influence the work reported in this paper.

Appendix B. Supplementary data

Supplementary data to this article can be found online at https://doi.

org/10.1016/j.jmrt.2025.12.121.

References

[1] Jaffery SHI, Khan M, Ali L, Mativenga PT. Statistical analysis of process parameters in micromachining of Ti-6Al-4V alloy. Proc Inst Mech Eng B J Eng Manuf 2016;230(6):1017–34. https://doi.org/10.1177/0954405414564409.

[2] Venkatesh V, Swain N, Srinivas G, Kumar P, Barshilia HC. Review on the machining characteristics and research prospects of conventional microscale machining operations. Mater Manuf Process 2017;32(3):235–62. https://doi.org/10.1080/10426914.2016.1151045.

[3] Kizhakken V, Mathew J. Modeling of burr thickness in micro-end milling of Ti6Al4V. Proc Inst Mech Eng B J Eng Manuf 2018;233(4):1087–102. https://doi.org/10.1177/0954405418769916.

[4] Chae J, Park SS, Freiheit T. Investigation of micro-cutting operations. Int J Mach Tools Manuf 2006;46(3–4):313–32. https://doi.org/10.1016/j.ijmachtools.2005.05.015.

[5] Özel T, Thepsonthi T, Ulutan D, Kaftanoğlu B. Experiments and finite element simulations on micro-milling of Ti-6Al-4V alloy with uncoated and cBN coated micro-tools. CIRP Ann Manuf Technol 2011;60(1):85–8. https://doi.org/10.1016/j.cirp.2011.03.087.

[6] Ali MY, Khan AA, Asharaf ABM, Wahab AA. Prediction of minimum chip thickness in tool based Micro end milling. Int J Integr Eng 2012;4(1):6–10.

[7] Thepsonthi T, Özel T. Experimental and finite element simulation based investigations on micro-milling Ti-6Al-4V titanium alloy: effects of cBN coating on tool wear. J Mater Process Technol 2013;213(4):532–42. https://doi.org/10.1016/j.jmatprotec.2012.11.003.

[8] Chen N, Li HN, Wu J, Li Z, Li L, Liu G, et al. Advances in micro milling: from tool fabrication to process outcomes. Int J Mach Tools Manuf 2021;160:103670. https://doi.org/10.1016/j.ijmachtools.2020.103670.

[9] Thepsonthi T, Özel T. Multi-objective process optimization for micro-end milling of Ti-6Al-4V titanium alloy. Int J Adv Manuf Technol 2012;63(9–12):903–14. https://doi.org/10.1007/s00170-012-3980-z.

[10] Nagesha BK, Dhinakaran V, Varsha Shree M, Manoj Kumar KP, Jagadeesha T. A review on weldability of additive manufactured titanium alloys. Mater Today Proc 2020;33:2964–9. https://doi.org/10.1016/j.matpr.2020.02.899.

[11] Venkata Rao K. A study on performance characteristics and multi response optimization of process parameters to maximize performance of micro milling for Ti-6Al-4V. J Alloys Compd 2019;781:773–82. https://doi.org/10.1016/j.jallcom.2018.12.105.

[12] Yadav R, Chakladar ND, Paul S. Modelling and experimental validation of burr control in micro milling of metals. Mater Today Commun 2023;35:106205. https://doi.org/10.1016/j.mtcomm.2023.106205.

[13] Chen MJ, Ni HB, Wang ZJ, Jiang Y. Research on the modeling of burr formation process in micro-ball end milling operation on Ti-6Al-4V. Int J Adv Manuf Technol 2012;62(9–12):901–12. https://doi.org/10.1007/s00170-011-3865-6.

[14] Rehman GU, Jaffery SHI, Khan M, Ali L, Khan A, Butt SI. Analysis of burr formation in low speed micro-milling of titanium alloy (Ti-6Al-4V). Mech Sci 2018;9(2):231–43. https://doi.org/10.5194/ms-9-231-2018.

[15] Bandapalli C, Singh KK, Sutaria BM, Bhatt DV. Experimental investigation of top burr formation in high-speed micro-end milling of titanium alloy. Mach Sci Technol 2018;22(6):989–1011. https://doi.org/10.1080/10910344.2018.1449213.

[16] Karakılınç U, Ergene B, Yalçın B, Aslantaş K, Erçetin A. Comparative analysis of minimum chip thickness, surface quality and burr Formation in micro-milling of wrought and selective laser melted Ti64. Micromachines 2023;14(6):1160. https://doi.org/10.3390/mi14061160.

[17] Jaffery SI, Mativenga PT. Assessment of the machinability of Ti-6Al-4V alloy using the wear map approach. Int J Adv Manuf Technol 2009;40(7–8):687–96. https://doi.org/10.1007/s00170-008-1393-9.

[18] Kim DH, Lee P-H, Lee SW. Experimental Study on machinability of Ti-6Al-4V in Micro end-milling. In: Proc World Congress on Engineering (WCE 2014). London, UK: Newswood Ltd; 2014. p. 962–6 (Lecture Notes in Engineering and Computer Science).

[19] Mhamdi M-B, Boujelbene M, Bayraktar E, Zghal A. Surface integrity of titanium alloy Ti-6Al-4V in ball end milling. Phys Procedia 2012;25:355–62. https://doi.org/10.1016/j.phpro.2012.03.096.

[20] Ezugwu EO, Wang ZM. Titanium alloys and their machinability—a review. J Mater Process Technol 1997;68(3):262–74. https://doi.org/10.1016/S0924-0136(96)00030-1.

[21] Veiga C, Davim JP, Loureiro AJR. Review on machinability of titanium alloys: the process perspective. Rev Adv Mater Sci 2013;34(2):148–64.

[22] Mian AJ, Driver N, Mativenga PT. A comparative study of material phase effects on micro-machinability of multiphase materials. Int J Adv Manuf Technol 2010;50(1–4):163–74. https://doi.org/10.1007/s00170-009-2506-9.

[23] Tan R, Madathil AP, Liu Q, Cheng J, Lin F. A hybrid GRA-TOPSIS-RFR optimization approach for minimizing burrs in micro-milling of Ti-6Al-4V alloys. Micromachines 2025;16(4):464. https://doi.org/10.3390/mi16040464.

[24] Lee K, Dornfeld DA. Micro-burr formation and minimization through process control. Precis Eng 2005;29(2):246–52. https://doi.org/10.1016/j.precisioneng.2004.09.002.

[25] Yabo Z, Qingshun B, Yangyang S, Donghai L. Burr formation mechanism and machining parameter effect in slot micro-milling titanium alloy Ti6Al4V. Int J Adv Manuf Technol 2022;123(5–6):2073–86. https://doi.org/10.1007/s00170-022-10298-w.

[26] Fang FZ, Liu YC. On minimum exit-burr in micro cutting. J Micromech Microeng 2004;14(7):984–8. https://doi.org/10.1088/0960-1317/14/7/020.

[27] Wu Y, Chen N, Bian R, He N, Li Z, Li L. Investigations on burr formation mechanisms in Micro milling of high-aspect-ratio titanium alloy Ti-6Al-4V structures. Int J Mech Sci 2020;185:105884. https://doi.org/10.1016/j.ijmecsci.2020.105884.

[28] Yadav R, Chakladar ND, Paul S. Micro-milling of Ti-6Al-4V with controlled burr formation. Int J Mech Sci 2022;231:107582. https://doi.org/10.1016/j.ijmecsci.2022.107582.

[29] Schueler GM, Engmann J, Marx T, Haberland R, Aurich JC. Burr formation and surface characteristics in micro-end milling of titanium alloys. Burrs - Analysis, control and removal. Berlin: Springer; 2010. p. 129–38. https://doi.org/10.1007/978-3-642-00568-8_14.

[30] Kiswanto G, Zariatin DL, Ko TJ. The effect of spindle speed, feed-rate and machining time to the surface roughness and burr formation of Aluminum Alloy 1100 in micro-milling operation. J Manuf Process 2014;16(4):435–50. https://doi.org/10.1016/j.jmapro.2014.05.003.

[31] Lekkala R, Bajpai V, Singh RK, Joshi SS. Characterization and modeling of burr formation in micro-end milling. Precis Eng 2011;35(4):625–37. https://doi.org/10.1016/j.precisioneng.2011.04.007.

[32] Yadav AK, Kumar M, Bajpai V, Singh NK, Singh RK. FE modeling of burr size in high-speed micro-milling of Ti6Al4V. Precis Eng 2017;49:287–92. https://doi.org/10.1016/j.precisioneng.2017.02.017.

[33] Özel T, Olleak A, Thepsonthi T. Micro milling of titanium alloy Ti-6Al-4V: 3-D finite element modeling for prediction of chip flow and burr formation. Prod Eng Res Devel 2017;11(4–5):435–44. https://doi.org/10.1007/s11740-017-0761-4.

[34] Aslantas K, Ekici E, Çiçek A. Optimization of process parameters for micro milling of Ti-6Al-4V alloy using Taguchi-based gray relational analysis. Measurement 2018;128:419–27. https://doi.org/10.1016/j.measurement.2018.06.066.

[35] Zheng L, Chen W, Huo D. Experimental investigation on burr formation in vibration-assisted micro-milling of Ti-6Al-4V. Proc Inst Mech Eng C J Mech Eng Sci 2018;233(12):4112–9. https://doi.org/10.1177/0954406218792360.

[36] Song W, Zhao M, Zhu J, Xue B, Wang H. Burr formation mechanism and experimental research in longitudinal-torsional ultrasonic-assisted milling Ti-6Al-4 V. Int J Adv Manuf Technol 2024;132:2315–31. https://doi.org/10.1007/s00170-024-13494-y.

[37] Kumar M, Bajpai V. Experimental investigation of top burr formation in high-speed micro-milling of Ti6Al4V alloy. Proc Inst Mech Eng B J Eng Manuf 2019;234(4):730–8. https://doi.org/10.1177/0954405419883049.

[38] Zheng X, Liu Z, Chen M, Wang X. Experimental study on micro-milling of Ti6Al4V with minimum quantity lubrication. Int J Nanomanuf 2013;9(5–6):570–82. https://doi.org/10.1504/IJNM.2013.057600.

[39] Vazquez E, Gomar J, Ciurana J, Rodríguez CA. Analyzing effects of cooling and lubrication conditions in micromilling of Ti6Al4V. J Clean Prod 2015;87:906–13. https://doi.org/10.1016/j.jclepro.2014.10.016.

[40] Ziberov M, da Silva MB, Jackson M, Hung WNP. Effect of cutting fluid on micromilling of Ti-6Al-4V titanium alloy. Procedia Manuf 2016;5:332–47. https://doi.org/10.1016/j.promfg.2016.08.029.

[41] Kumar A, Bhagat KC, Gangopadhyay S, Das P. Effect of flow rate in minimum quantity lubrication (MQL) in micro-drilling of Ti-6Al-4V. Int J Adv Manuf Technol 2024;135(11–12):5173–86. https://doi.org/10.1007/s00170-024-14756-5.

[42] Aslantas K, Çicek A, Ucun I, Percin M, Hopa HE. Performance evaluation of a hybrid cooling-lubrication system in micro-milling of Ti6Al4V alloy. Proced CIRP 2016;46:492–5. https://doi.org/10.1016/j.procir.2016.04.037.

[43] Kim JS, Kim JW, Lee SW. Experimental characterization on micro-end milling of titanium alloy using nanofluid minimum quantity lubrication with chilly gas. Int J Adv Manuf Technol 2017;91(5–8):2741–9. https://doi.org/10.1007/s00170-016-9965-6.

[44] Khaliq W, Zhang C, Jamil M, Khan AM. Tool wear, surface quality, and residual stresses analysis of micro-machined additive manufactured Ti–6Al–4V under dry and MQL conditions. Tribol Int 2020;151:106408. https://doi.org/10.1016/j.triboint.2020.106408.

[45] Khosravi J, Azarhoushang B, Barmouz M, Bösinger R, Zahedi A. High-speed milling of Ti6Al4V under a supercritical CO2 + MQL hybrid cooling system. J Manuf Process 2022;82:1–14. https://doi.org/10.1016/j.jmapro.2022.07.061.

[46] Zhecheva A, Sha W, Malinov S, Long A. Enhancing the microstructure and properties of titanium alloys through nitriding and other surface engineering methods. Surf Coat Technol 2005;200(7):2192–207. https://doi.org/10.1016/j.surfcoat.2004.07.115.

[47] Banerjee D, Williams JC. Perspectives on titanium science and technology. Acta Mater 2013;61(3):844–79. https://doi.org/10.1016/j.actamat.2012.10.043.

[48] Ziberov M, de Oliveira D, da Silva MB, Hung WNP. Wear of TiAlN and DLC coated microtools in micromilling of Ti-6Al-4V alloy. J Manuf Process 2020;56(A):337–49. https://doi.org/10.1016/j.jmapro.2020.04.082.

[49] Ross PJ. Taguchi techniques for quality engineering. second ed. New York: McGraw-Hill; 1996.

[50] Aslantas K, Haşçelik A, Erçetin A, Danish M, Alatrushi LKH, Rubaiee S, et al. Effect of cutting conditions on tool wear and wear mechanism in micro-milling of additively manufactured titanium alloy. Tribol Int 2024;193:109340. https://doi.org/10.1016/j.triboint.2024.109340.

[51] Rehan M, He T, Khalil AK, Tahir D, Yip WS, To SS. Experimental investigation of the micro-milling of additively manufactured titanium alloys: selective laser melting and wrought Ti6Al4V. Chin J Mech Eng 2024;37:136. https://doi.org/10.1186/s10033-024-01139-w.

[52] Abbasi–Nahr M, Mirsalehi SE. Additive friction stir deposition of AA5083/MoS2-diamond hybrid nanocomposites: investigating their metallurgical, mechanical,

tribological, and electrochemical characteristics, and process-structure-property relationships. J Alloys Compd 2025;1013:178553. https://doi.org/10.1016/j.jallcom.2025.178553.

[53] Razmjoo H, Mirsalehi SE, Abbasi-Nahr M, Navidi-Helan M. Microstructure, corrosion, and tribological performance of multilayered cylindrical AA5083 parts fabricated by modified friction stir deposition – additive manufacturing. Mater Charact 2025;221:114777. https://doi.org/10.1016/j.matchar.2025.114777.

[54] Abbasi-Nahr M, Mirsalehi SE, Mirhosseini SS. Additive manufacturing of AA5083/TiN-Diamond hybrid nanocomposite parts via additive friction stir deposition: metallurgical structure, mechanical, tribological, and electrochemical properties. J Mater Res Technol 2024;30:8187–208. https://doi.org/10.1016/j.jmrt.2024.05.158.

[55] Abbasi Nahr M, Mirsalehi SE, Papi A. Additive manufacturing of AA2024/Al2O3 nanocomposites via friction surfacing: investigating metallurgical, mechanical, and tribological properties. J Mater Res Technol 2025;36:8609–31. https://doi.org/10.1016/j.jmrt.2025.05.124.

[56] Chen G, Gao Q, Yang X, Liu J, Su Y, Ren C. Investigation of heat partition and instantaneous temperature in milling of Ti-6Al-4V alloy. J Manuf Process 2022;80:302–19. https://doi.org/10.1016/j.jmapro.2022.05.051.

[57] Langenhorst L, Sölter J, Heinzel C. Partitioning of primary shear zone heat in face milling. CIRP Ann Manuf Technol 2022;71(1):53–6. https://doi.org/10.1016/j.cirp.2022.04.010.

[58] Joo J, Kim J, Yang SM, Park HW, Kim DY. Tool wear evolution and chip formation of the Ti-6Al-4V end milling under cryogenic cooling and minimum quantity lubrication conditions. Int J Adv Manuf Technol 2024;130:589–602. https://doi.org/10.1007/s00170-023-12704-3.

[59] Baig A, Jaffery SHI, Khan MA, Alruqi M. Statistical analysis of surface roughness, burr formation and tool wear in high speed micro milling of inconel 600 alloy under cryogenic, wet and dry conditions. Micromachines 2023;14(1):13. https://doi.org/10.3390/mi14010013.

[60] Shokrani A, Dhokia V, Newman ST. Environmentally conscious machining of difficult-to-machine materials with regard to cutting fluids. Int J Mach Tools Manuf 2012;57:83–101. https://doi.org/10.1016/j.ijmachtools.2012.02.002.

[61] Liu X, DeVor RE, Kapoor SG, Ehmann KF. The mechanics of machining at the microscale: assessment of the current state of the science. J Manuf Sci Eng 2004;126(4):666–78. https://doi.org/10.1115/1.1813469.

[62] Bissacco G, Hansen HN, De Chiffre L. Size effects on surface generation in Micro milling of hardened tool steel. CIRP Ann Manuf Technol 2006;55(1):593–6. https://doi.org/10.1016/S0007-8506(07)60490-9.